Influence of synkinematic sedimentation in a thrust system with two decollement levels; analogue modelling

T. Pichot, Thierry Nalpas

Tectonophysics
August 2009, Volume 473, Issues 3-4, Pages 466-475
http://dx.doi.org/10.1016/j.tecto.2009.04.003

Influence of synkinematic sedimentation in a thrust system with two decollement levels; analogue modelling

T. Pichot[a, b] and T. Nalpas[a, *]

[a] Géosciences Rennes, Université de Rennes 1, UMR 6118 Campus de Beaulieu, 35042 Rennes cedex, France
[b] Ifremer, Centre de Brest, Z.I. Pointe du Diable, B.P. 70, 29280 Plouzané, France

*: Corresponding author : T. Nalpas, Tel.: +33 223235675; fax: +33 223236100, email address : thierry.nalpas@univ-rennes1.fr

Abstract:

Compressive systems in foreland domains are characterised by fold and thrust belts linked to the presence of one or several ductile layers in depth acting as a decollement level. The main parameters controlling the structural evolution are: the presence of a decollement level, the amount and rate of shortening, and the amount of synkinematic sedimentation. The effect of these parameters has only been studied on a thrust belt scale. Furthermore, only the effect of synkinematic sedimentation on a simple system with one decollement level has been studied at the scale of a single structure. The aim of this study was to use analogue modelling to test the effect of shortening rate, velocity and the localization of sedimentation on a single system characterised by the presence of two prekinematic decollement levels. The main results showed variations in the structural vergence, folding geometry (symmetric or asymmetric), the evolution of the deformation (horizontal propagation versus vertical uplift), and the decoupling of the lower and upper brittle structures in relation with the main parameters (shortening rate and mass transfer). The results of the experiments were then compared to natural examples from the sub-Andean thrust belt.

Keywords: Thrust; Decollement level; Synkinematic sedimentation; Analogue modeling

Introduction

In a compressive system, and especially in a thin-skinned thrust belt, a deformation induced by one or several decollement levels is commonly observed (e.g. flat, ramp, fault-related folding). Decollement levels present a low basal friction directly related to the lithology (marls, shales, coals and evaporites) and/or to overpressure conditions. The Sub-Andean fold and thrust-belt shows a major west-to-east propagation of the deformation (Fig. 1). This deformation is characterised by north-south folds-faults (Fig. 1b) and is related, in depth, to two decollement levels (Fig. 1c). These structures, which developed during sedimentation, present mostly a west-to-east vergence with a huge horizontal and vertical displacement. Previous analogue studies have investigated the entire scale of the thrust-belt (Leturmy et al., 2000; Couzens-Schulz et al., 2003; Smit et al., 2003). The main characteristics of this system are the basal angle of the wedge and the shortening rate, which control the propagation of the thrust sequences (Smit et al., 2003). The presence of two decollement levels favours either coupling or decoupling, related to the shortening rate (Couzens-Schulz et al., 2003; Massoli et al., 2006). The presence of synkinematic sedimentation modifies the thrust wavelength and the major propagation of the deformation (Leturmy et al., 2000). On a structural scale, only a few studies have addressed the relationship between deformation and sedimentation using analogue modelling (Nalpas et al., 1999; Casas et al., 2001; Barrier et al., 2002; Nalpas et al.; 2003; Gestain et al., 2004). All of these studies were carried out with only one prekinematic ductile layer and showed an increase in the uplift associated with the sedimentation rate. At the scale of a single structure with two prekinematic ductile layers, the vergence of thrust, the localization of deformation, the relation between structuration in depth and at the surface, and the effect of mass transfer are still in debate.

The aim of this paper is to study the deformation of a structure in a domain presenting two prekinematic decollement levels in relation to the (i) shortening rate variation, (ii) synkinematic velocity of the sedimentation and (iii) localization of the synkinematic sedimentation. Our approach was based on analogue modelling and field examples (e.g. Sub-Andean thrust-belt).

2. Experimental procedure

The modelling techniques used here are similar to those usually used for experiments dealing with brittle-ductile systems in the Laboratory of Experimental Tectonics of Géosciences Rennes (Rennes University, FRANCE) and which have been described in numerous studies (e.g. Faugère and Brun 1984; Vendeville et al. 1987; Davy and Cobbold 1991). Brittle layers (pre and synkinematic) were represented by sand, with an angle of internal friction close to 30° (Krantz, 1991) and a density (ρ) around 1,400 kg/m3. Weak ductile layers such as shales, clay, marl or salt were represented by two

silicone putties (Rhône Poulenc, France) with a viscosity (μ) around 10^5 Pa.s at 20°C and a density (ρ) close to 1,400 kg/m3 for the silicone putty 70 009, and a viscosity (μ) around 10^4 Pa.s at 20°C and a density (ρ) close to 1,000 kg/m3 for the transparent silicone putty SGM 36.

The experimental apparatus consisted of a fixed rigid basal plate over which a thin mobile plate fixed on a mobile wall was pushed at a constant rate (Fig. 2a). The shape of the mobile plate induces a velocity discontinuity (VD) at the base of the model, which localises the deformation (cf. Malavielle 1984; Balé 1986; Allemand et al. 1989; Ballard 1989). The model was set in a 70 x 60 cm sandbox, wide enough to achieve a relatively large amount of shortening without border effects.

In order to make comparisons with natural examples, where the thickness of the ductile and brittle layers are different from the base to the top of the sedimentary pile of the basin, we chose a four-layer brittle-ductile model with ductile and brittle material that is thicker in the lowermost layers than in the uppermost layers. The prekinematic pile of the models was made of a four-layer brittle-ductile system, composed of, from bottom to top: 1 cm of either pink or purple silicone; 1.5 cm of black and white sand; 0.5 cm of transparent silicone; and 1cm of black and white sand (see Fig. 2a). The basal and the medium silicone layers represent potential decollement levels, while the sand layers represent brittle prekinematic formations. Several shortening rates, ranging from 0.25 to 10 cm/h, were tested, and a rate of 0.5 cm/h was kept for the experiment. The geometric and dynamic scaling of these models was presented in Table 1. The scale ratio and stress ratio between model and nature has the same order (10^{-5}), and the velocity in the model corresponds to observed velocity in nature (see Table 1).

In order to simulate synkinematic sedimentation, fresh sand was continuously sprinkled manually onto the model during the shortening (Barrier et al., 2002). The sedimentation modes (Fig. 2b) were chosen to constrain the possible sedimentation modes within natural basins (see § 3.2, below). Photographs of the model surface were taken at regular time intervals in order to observe structure development. After deformation, the internal structure was observed on a series of cross-sections cut parallel to the compression direction (perpendicular to the VD). Brittle sand layers were made of various colours of sand in order to reveal the structures and to observe them on photographs. The colour of the sand does not modify its behaviour.

3. Analogue results

3.1. Shortening rate variation

The first aim of our experiments was to test several shortening rates in order to define the best rate to match thin-skinned tectonic features (e.g. flat, ramp, fault-related folding) unaffected by the influence of

the experimental apparatus. Six different shortening rates were applied to the model: 0.25, 0.5, 1, 2.5, 5 and 10 cm/h. We first tested 5 cm of shortening, followed by 10 cm of shortening. In this paper, we present the results obtained with 3 shortening rates (0.5, 1 and 5 cm/h; Fig. 3).

It was possible to define the global geometries in all of the experiments. The deformation corresponded to an uplift with an anticline shape, and which was always located above the linear velocity discontinuity (VD). According to the definition of VD and the induced shear displacement (Ballard, 1989), a synthetic reverse fault occurs when the hanging wall moves toward the mobile plate. On the contrary, an antithetic reverse fault is characterised by the hanging wall moving in an opposite direction to the mobile plate. The lower brittle layer was always characterised by a major reverse fault with flat and ramp geometry. This basal structure had an average ramp angle of 25° (Fig. 3). The major deformation of the upper brittle layer was located above the major basal deformation in the lower brittle layer. The major basal reverse faults in the lower brittle layer and the major reverse faults in the upper brittle layer were associated with a sheet of silicone at the base of the hanging wall. In the upper brittle layer, the vergence of the reverse fault was the same as seen for the reverse fault in the basal brittle layer. In order to obtain a fault displacement with the same vergence in the lower and upper brittle layers, it is necessary to have an opposite sense of shear in the upper ductile layer, as is observed in the brittle layers. This opposite sense of shear is characteristic of fish tail structures described in nature (Meneley, 2006). In all the experiments, the frontward or backward propagation was related to development of the structures, with regard to the major lower brittle layer fault. Thus, a development of structures above the footwall of the lower major fault corresponded to a frontward propagation, while a development of structures above the hanging wall of the lower major fault corresponded to a backward propagation.

3.1.1. 5 cm/h of shortening rate

In this experiment, the global geometry was strongly symmetrical throughout the entire model (Fig. 3a), and the structure looked like a box-fold or pop-up structure. The lower brittle layer was characterised by the presence of a major synthetic reverse fault (with regard to the mobile plate). This fault was composed of two segments that defined a horizontal throw (flat) and a high dip vertical throw (ramp). The major synthetic reverse fault was associated with a conjugate minor fault. Two faults formed in the upper brittle layer which were directly linked to the lower brittle layer deformation and presented a flat geometry.

126 *3.1.2. 1 cm/h of shortening rate*

127 The global geometry was asymmetrical (Fig. 3b), and the structure looked like a fault-bend fold. The
128 lower brittle layer was characterised by a well-developed major synthetic reverse fault (with regard to
129 the mobile plate), associated with a very weak conjugate minor reverse fault. The hanging wall of this
130 major fault generated a wedge which was underthrusting within the upper ductile layer. In the upper part
131 of the model, the deformation was accommodated by reverse fault systems related to this wedge. The
132 upper silicone layer acted as a passive roof thrust and as a decollement level for the uppermost structural
133 level (Bonini, 2001; 2003). The upper brittle layer deformation propagated frontward: first, with a small
134 tilted asymmetric pop-up structure located above the basal major synthetic reverse fault, and then, with
135 a small pop-up structure.

136

137 *3.1.3. 0.5 cm/h of shortening rate*

138 The global geometry was strongly asymmetrical (Fig. 3c), and the structure looked like a fault-bend
139 fold. The deformation style evolved with a frontward propagation. The lower brittle level was
140 characterised by a well-developed major antithetic reverse fault (with regard to the mobile plate). At this
141 shortening rate, there were no conjugate fault systems in the lower brittle layer. The upper brittle layer
142 deformation propagated frontward: first, with a planar reverse fault, and then, with a steep reverse fault
143 with the same vergence of the lower major brittle fault. In the upper brittle layer, a fault propagation
144 fold accommodated the shortening. The whole deformation was comparable to an active-roof duplex
145 (Couzens-Schultz et al., 2003).

146

147 *3.1.4. Influence of shortening rate*

148 Based on our experiments, we built strain profiles (in compression where $\sigma v = \sigma 3$) based on the brittle
149 (Sb) and ductile (Sd) strength. Thus, we were able to use the brittle and ductile strength ratio (SR = Sb/
150 Sd), which has either a high or low value (see Annex 1).

151 At 5 cm/h (i.e. a weak SR), the deformation style in the upper and lower brittle layers was linked by the
152 middle ductile layer (see § 3.1.1. above). At this shortening rate, the resistance of the middle ductile
153 layer did not allow for an efficient decollement level between the two brittle layers, and instead,
154 favoured a coupled deformation (see Annex 1). The global geometry was not dominated either by the
155 brittle or ductile layers, and the shortening was accommodated by diffused deformation (i.e. a
156 symmetrical global geometry with a pop-up shape).

At 1 cm/h, the deformation style in both the upper and lower brittle layers was not completely decoupled. The middle ductile layer promoted a frontward propagation of the deformation in the uppermost sand layer, as seen in the experiment with a shortening rate of 0.5 cm/h. As in the experiment with a shortening rate of 5 cm/h, a very weak conjugate minor reverse fault in the lower brittle layer was associated with a fault in the upper brittle layer. A transitional behaviour was observed at this shortening rate.

At 0.5 cm/h (i.e. a strong SR), the deformation recorded in the upper brittle layer was decoupled from the lower one (see § 3.1.3. above). Because of a weak Sd and therefore, a high stress ratio (SR) value, the middle ductile layer became an efficient decollement level. The brittle sand layers were then decoupled. A frontward propagation of the localised deformation occurred and consequently, an asymmetrical geometry developed.

Six different shortening rates were tested (from 0.25 to 10 cm/h). We decided to retain a shortening rate of 0.5 cm/h because: (i) the structure created in the lower brittle layer was either a synthetic or an antithetic reverse fault (with regard to the mobile plate), meaning that the basal silicone putty acted as an efficient decollement; (ii) a frontward propagation was developed in the upper brittle layer, meaning that the silicone putty acted as an efficient decollement level between the two brittle layers; (iii) shortening was accommodated by propagation folding and faulting, according to real thin-skinned fold-and-thrust belts evolutions and (iv) according to the scaling of our experiments (see Table 1).

3.2. Homogeneous synkinematic sedimentation

In order to represent synkinematic sedimentation, sand was continuously sprinkled horizontally on the top of the model during the deformation (alternating between a blue and white colour). The sedimentation velocity was based on the most common rates observed in nature (Fig. 4). We used the following ratio to define this rate: $R = Vs / Vu$, where R is the ratio between the velocity of the sedimentation (Vs) and the velocity of the structure uplift (Vu) (see Barrier et al., 2002). In a natural environment, it is possible to recognise four main situations related to the type of sedimentation in relation with the base level and the variation of accommodation space situated below: 1) no creation of accommodation space and then, no sedimentation (here, the ratio R is equal to 0); or 2) less creation of accommodation space than creation of topography, and thus, less sedimentation than uplift ($0 < R < 1$); 3) the same amount of creation of accommodation space as creation of topography, and consequently, the same amount of sedimentation as uplift ($R = 1$); or 4) more creation of accommodation space than creation of topography, and thus more sedimentation than uplift ($R > 1$). In our experiments, we only

tested the influence of sedimentation without erosion, and our R ratio ranged from 0 to 2 (Fig. 4). In order to estimate Vs and Vu, we manually measured the difference between the topography of the experiment and a fixed point at a regular time interval. This evolution was checked on a cross-section at the end of the experiment.

In general, the upper and lower structures were superimposed (see Fig. 5) and had the same vergence (except in Fig. 5a4). The lower brittle layer was characterised by a flat and ramp geometry with a very weak vertical throw, in contrast with the uplifted upper structures. The synkinematic brittle layers followed the deformation of the upper prekinematic brittle layer. From the bottom to the top, we observed a progressive decrease of dip in the synkinematic layers. The homogeneous synkinematic sedimentation located in the hanging wall was deformed and pinched out toward the thrust system while in the footwall, the thickness of the sediments was more constant with a flatter geometry. The major basal reverse faults in the lower brittle layer and the major reverse faults in the upper brittle layer were associated with a sheet of silicone at the base of the hanging wall, as seen in the experiment without sedimentation (Fig. 3). The silicone layers were thicker at the base of the ramp, in both the lower and upper ductile layers, and also at the front of the hanging wall wedge in the upper ductile layer.

3.2.1. 5 cm of shortening

For R = 3/4 and R = 1, the major influence of the homogeneous synkinematic sedimentation was to generate a single major thrust in the uppermost brittle layer (Figs. 5a2, 5a3). The throw and angle of this major thrust increases with an increasing R (see Barrier et al., 2002). For R = 2, several faults were created in the uppermost brittle layer (Fig. 5a4). This means that at a low sedimentation velocity (R=3/4, and R = 1), a flexural deformation prevails, while at a high sedimentation velocity (R=2), brittle deformation is predominant (Nalpas et al., 1999). In the present study, the lower brittle layer was characterised by a well-developed fault-bend fold without a conjugate fault. At a high R, the major basal thrust evolved into a well-developed flat hanging wall.

3.2.1.1. R = 0. Please refer to § 3.1.3. and Fig. 3c.

3.2.1.2. R = 3/4. The lower structure was characterised by a major antithetic thrust (with regard to the mobile plate) with an angle of 15° (Fig. 5a2). In the upper prekinematic brittle layer, one reverse fault (with the same vergence of the thrust in the lower brittle layer) was developed with an average angle of

18°, and with a ramp anticline in the hanging wall. This fault kept growing throughout the synkinematic upper brittle layers without a significant change in the dip.

3.2.1.3. R = 1. The basal structure was characterised by a major antithetic thrust (with regard to the mobile plate) with a ramp angle of 13° (Fig. 5a3). In the upper prekinematic brittle layer, one thrust was developed with an average angle of 21° (with the same vergence of the thrust in the lower brittle layer). This fault kept growing throughout the synkinematic brittle layer with an increasing dip up to 63° (see Barrier et al., 2002). A large sheet of silicone was preserved between the footwall and the hanging wall of this structure. The crest of this structure was very narrow, while the flanks were steeped. Note that in the upper brittle layer, the deformation was associated with vertical displacement and uplift, while in the lower brittle layer, the deformation was associated with horizontal displacement.

3.2.1.4. R = 2. The basal structure was characterised by a major antithetic thrust (with regard to the mobile plate) with a ramp angle of 11° (Fig. 5a4). In the upper prekinematic brittle layer, one major reverse fault (with an opposite vergence to the thrust in the lower brittle layer) was developed with an average angle of 35° at the base, and was divided into two segments with a dip that progressively increased its dip in the synkinematic brittle layers, up to 47° at the top. A conjugate reverse fault was developed in its hanging wall during sedimentation of synkinematic brittle layers and stopped progressively. A newly formed reverse fault was created in the synkinematic brittle layers during the last stages of deformation. This fault was located in the footwall of the major reverse fault that developed in the upper brittle layers, and was ramified to the base of this major reverse fault. In contrast with the previous experiment, the deformation of synkinematic brittle layers did not show flexure with a significant variation in layers dip.

3.2.2. 10 cm of shortening

3.2.2.1. R = 0. The vertical colours in the lower silicone layer were only used as passive markers in order to analyse the deformation. The lower brittle layer was characterised by a major synthetic reverse fault (with regard to the mobile plate, see § 3.1.4) with a significant horizontal throw creating a large hanging wall flat (Fig. 5b1). The curvature of the hanging wall associated with the thrust was less significant than seen in the previous experiment, and produced a large deformation. The upper sand layer was affected by a large domain of a complex deformation characterised by synthetic and antithetic reverse faults, fault-propagation fold and detachment fold, localised in both the hanging wall and the

footwall of the basal thrust. In the footwall domain, the deformation recorded a stronger shortening than observed in the hanging wall domain, as illustrated by the pop-down structure. Just above the lower thrust, extensional structures were developed and were associated with the uplift of silicone (diapiric effect).

3.2.2.2. R = 3/4. The deformation was complex in the lower brittle level. One major antithetic thrust (with regard to the mobile plate) was developed first, with a significant horizontal throw creating a large hanging wall flat (Fig. 5b2). A conjugate high dipping minor reverse fault was developed during the last stage of the deformation. The upper silicone layer was cut by the uplift of the lower brittle layer in the direction of the base of the upper prekinematic brittle layer, related to the movement on the basal faults. The base of the upper structure was gently symmetrical and evolved into a more complex deformation toward the top. A first reverse fault was developed during the early stage of the deformation, with an opposite vergence to the major thrust in the lower brittle layer. A second high dipping reverse fault, with the same vergence to the major thrust in the lower brittle layer, cut the first one. The deformation of the synkinematic brittle layers showed the same flexure in both the hanging wall and footwall.

3.2.2.3. R = 1. A major synthetic thrust (with regard to the mobile plate) developed at the base of the model (Fig. 5b3). This thrust showed a horizontal hanging wall ramp, like a flat geometry, and a dip hanging wall flat, like a ramp geometry. A conjugate high dipping minor reverse fault was developed during the last stage of the deformation. The upper silicone layer was cut by the uplift of the lower brittle layer in the direction of the base of the upper prekinematic brittle layer, related to the movement on the basal faults. In the upper part of the model, the shortening was accommodated by a huge reverse fault (with the same vergence to the major thrust in the lower brittle layer) with an angle of 31° at the base, and which evolved upward to 59° in the synkinematic brittle layers.

3.3. Local synkinematic sedimentation

For the sedimentation in these experiments, we used the same method as in the homogeneous synkinematic sedimentation. However, synkinematic sedimentation (R = 1) was deposed only on the footwall or only on the hanging wall, respectively, with the lower brittle thrust geometry (Fig. 6). In Figure 6, all the experiments were presented with the same basal brittle thrust vergence so that in all cross-sections, the hanging wall of the lower brittle thrusted in the left side, and the footwall in the right side. This disposition of the experiments was presented in order to better compare the effect of the localised synkinematic sedimentation on the evolution of upper brittle layer deformation. Because we

had chosen a velocity that allows the development of a synthetic or antithetic reverse fault in the lower brittle layer, with regard to the mobile plate (see § 3.1.4), it was not a problem to change the position of the mobile plate.

The main characteristics observed were a well-developed major thrust in the lower brittle layer and several thrust propagations in the upper brittle layer, where synkinematic sedimentation was not applied.

3.3.1. Synkinematic sedimentation in the hanging wall domain

3.3.1.1. 5 cm of shortening. One thrust was developed in the lower brittle layer (Fig. 6a2). In the upper brittle level, the shortening was only accommodated in the domain with no sedimentation (footwall). The deformation propagated frontward (in the direction of the footwall, see § 3.1.) with the development of two reverse faults (with the same vergence as the basal thrust), the second fault with a major throw. The central part of the model, above the ramp anticline of the basal thrust, was characterised by an extensional zone, which was localised on the main anticline of the upper brittle layer.

3.3.1.2. 10 cm of shortening. With an increase in shortening, the deformation was accommodated by a greater number of more complex structures (Fig. 6b2). As already observed for a shortening of 5 cm, a major thrust is developed first in the lower brittle layer with a flat hanging wall, and then, a small reverse fault is developed frontward. In the upper brittle level, the shortening was only accommodated in the domain with no sedimentation (footwall). The deformation first propagated frontward with the development of two reverse faults with the same vergence as the basal thrust (the second one had the major throw). Then, the third structure was a small asymmetrical pop-up with an opposite vergence to the other structures. An extensional domain developed in the upper brittle layer, above the ramp anticline of the basal thrust, was affected the upper brittle layer.

3.3.2. Synkinematic sedimentation in the footwall domain

3.3.2.1. 5 cm of shortening. One thrust was developed in the lower brittle layer (Fig. 6a3). The hanging wall ramp of this thrust was uplifted, in contrast with the experiment with 5 cm of shortening, and sedimentation in the hanging wall domain (Fig. 6a2). Associated with this thrust, an anticline grew backward. The middle silicone was cut off by the contact between the uplifted basal thrust and the prekinematic upper brittle layer. In the upper brittle layer, the shortening was first accommodated by a step reverse fault located above the crest of the basal anticline, with the same vergence of this basal thrust, and then by two reverse faults which propagated backward, with an opposite vergence to the

basal thrust. The main basal structure defined an underthrusting wedge within the upper silicone layer, which acted as an active roof duplex and as a decollement level for the uppermost structural sequence.

3.3.2.2. 10 cm of shortening. Several thrusts developed in the lower brittle layer (Fig. 6b3). One major thrust associated with a huge anticline was developed, which was faulted at its crest with the same vergence. A second thrust developed backward with the same vergence. In the upper brittle layer, a complex deformation was localised in the hanging wall, and propagated backward with an oscillating vergence, with regard to the thrusts in the lower brittle level. The first reverse fault was created above the lower brittle ramp anticline, with the same vergence of the basal thrust, and then the over-structures (fault-propagation fold) were developed with an opposite vergence. The main basal structure was like a wedge inserted into the upper silicone layer, which acted as a passive roof thrust and as a decollement level for the uppermost structural sequence.

4. Discussion

4.1. Influence of homogeneous synkinematic sedimentation

The main observation of these experiments with homogeneous sedimentation, either with 5 cm or 10 cm of shortening, is the absence of frontward or backward propagation of the deformation in the upper brittle layer, contrary to the experiments performed without sedimentation, or with local sedimentation. This is directly related to the evolution of the strength profile in the upper brittle layer, and thus, is related to sedimentation (see Annex 1). When there is no sedimentation, the upper layer strength is the same everywhere in the model (Fig. 7a), and when there is sedimentation around the structure, the strength increases proportionally to the amount of sedimentation in the footwall and hanging wall (Fig. 7b).

The deformation in the upper brittle layer is concentrated in one major fault above the basal structure: the fault dip of this major fault increases progressively during sedimentation. This is also related to the effect of sedimentation and is in good agreement with Barrier et al. (2002).

In our experiments, we observed a large variation in the upward thrust dip linked to the ratio R and the amount of shortening in the upper brittle layer. In the experiment where R = 2, (e.g. with a high rate of sedimentation), the upper brittle layer strength increases very rapidly during the first stage of the deformation and favours a brittle behaviour. Consequently, we observed several reverse faults cutting the synkinematic brittle layer, with very low flexures between the faults.

In the lower brittle layer (for experiments with 5 cm of shortening), when the rate of sedimentation (R) is increasing, the thrust dip decreases from 15° (R = 3/4) to 11° (R = 2). The same trend is seen in the experiments with 10 cm of shortening. Related to the increase of R, the shortening in the lower brittle layer is accommodated by a horizontal evolution of the structure, while in the upper brittle layer, it is accommodated by a vertical evolution of the structure and uplift. This is directly related to the stress induced by sediment load. The horizontal movement of the basal structure produces a penetration of a wedge in the upper silicone layer (underthrusting), which induces a variation in thickness, with an increase at the basal fault front and a decrease over the frontal limb of the anticline.

4.2. Influence of local synkinematic sedimentation

The main observation of these experiments, either for 5 cm or 10 cm of shortening, is the absence of a propagation of the deformation in the upper brittle layer where sedimentation is applied, in contrary to the domain without sedimentation. This is in good agreement with the evolution of the strength profile in the upper brittle layer, related to sedimentation and brittle strength increases of the upper brittle layer (see Annex 1, Fig. 7c). Where there is no sedimentation, the upper brittle layer is not as strong than where there is sedimentation (Fig. 7c), and therefore, the deformation in the upper brittle layer is concentrated in the weakest zone, without sedimentation, or frontward or backward (with regard to the major basal structure).

The deformation of the lower brittle layer shows the same evolution as the upper brittle layer, with propagation of the deformation and creation of a new fault in the zone where there is no synkinematic sedimentation. This synkinematic sedimentation applied above the footwall, or above the hanging wall, promotes a forced decoupling between the upper and lower brittle layers where there is no sedimentation. The reason for this is the same as before: it is due to an increase in the lower brittle layer strength (Fig. 7c).

This means that sedimentation influences not only the evolution of the shape of one structure, but also the localisation of the deformation.

4.3. Comparison between field examples and analogue modelling

In the Tarija basin example, numerous compressive structures are developed in association with two superimposed decollement levels and sykinematic sedimentation. The vergence of these structures is mostly eastward. They are composed of a lower decollement level in the Silurian Kirusillas shales and a second decollement level in the Los Monos Devonian shales (Fig. 8). The deformation started at about

8.5-9 Ma with the formation of the El Pescado range and propagated eastward until 2.7 Ma, when the Arguarague range lift started (Echavarria et al., 2003). During this period, synkinematic sedimentation was accumulated, with a progressive decrease in thickness from west-to-east.

In the San Antonio Range example, a fault-bend fold was initiated in the Silurian shales and propagated upward throughout the upper competent units, with an eastward vergence, until reaching the upper incompetent layer (Devonian shales). The ramp anticline of this structure is cut by a second reverse fault, which is steeper than the major basal structure. The upper part of the San Antonio Range (from the Lower Permian to the Quaternary) is a more symmetric structure with a big vertical amplification (Fig. 8).

In the Arguaragüe Range example, the lower thrust was initiated in the Silurian shales and had a classic fault-bend fold geometry. The upper part of the Arguaragüe Range shows the development of a reverse fault, with the same vergence as the basal one. The main system is asymmetric with an eastward vergence.

From our modelling results, we suggest that synkinematic sedimentation was the major parameter to explain this variation in structure growth: (i) when synkinematic sedimentation velocity is low, the development of the structure is mainly asymmetric with an easy thrusting, like in Figure 5a2, and (ii) when synkinematic sedimentation velocity is high, the development of the structure is mainly symmetric with a more vertical growth, like in Figure 5a2.

The implication of these interpretations is that from west-to-east, in the case of the Tarija basin, the eastward decrease of the synkinematic sedimentation produces a large variation in compressive structures. This is directly applicable at the foreland basin scale to explain the evolution of the structure in the direction of the foreland (see Fig. 1c).

5. Conclusions

The main results are related to the rate of deformation, the velocity of synkinematic sedimentation, the localization of synkinematic sedimentation and the comparison with nature.

- The deformation rate strongly influences a change in deformation style in analogue modelling. At a high shortening rate, the strong resistance of the ductile layer does not allow for an efficient decollement level and favours a coupled and symmetric deformation. At a low shortening rate, the weak resistance of the ductile layer allows the decoupling between the brittle layers, and favours an asymmetrical deformation, with the creation of an active roof duplex.

This decoupling favours the flow of the silicone layers, generating variations in thickness which allows the system to accommodate the shortening, and then, produces an underthrust of the wedge within the upper silicone layer, and therefore, compensates for the brittle deformation.

- The main observations from the experiments with homogeneous sedimentation suggest: (i) with sedimentation, the deformation in the upper brittle layer cannot propagate either frontward or backward, in relation to strength increases, (ii) with the increase of sedimentation velocity, the fault dip of the major upper brittle fault increases progressively.
- With local sedimentation, the domain without sedimentation promotes the frontward or backward propagation of the deformation in both the upper and lower brittle layers. Within the sedimentation domain, synkinematic sedimentation inhibits the creation of such a structural evolution. The strength ratio between these two domains is not equal, and the deformation is localised where the resistance is weakest.
- As suggested by the Subandean natural examples, the variation of synkinematic sedimentation produces a large variation in compressive structures; asymmetric thrusting with low velocity synkinematic sedimentation, and mainly symmetric structure and vertical growth, with high velocity synkinematic sedimentation.

Annex 1:

Strength profiles

Previous works have analyzed the effects of brittle-ductile coupling in terms of relative strength between the brittle and ductile layers in compressive settings (Bonini, 2001; Smit et al., 2003). We have chosen to apply the same approach.

The vertical normal stress (σ_v) at the base of the brittle layers is given by

$$\sigma_v = \rho.g.Tb \qquad (1)$$

where ρ is the brittle layer density, g is the acceleration due to gravity and Tb is the thickness of the brittle layer. Because $\sigma_v = \sigma 3$ in compression, the maximum differential stress is

$$\sigma 1 - \sigma 3 = 2.\ \rho.g.Tb \qquad (2)$$

Thus, the maximum differential stress in the brittle layer is only controlled by the layer thickness (Tb) and its density (ρ).

The shear stress (τ) in the ductile layer is given by

$$\tau = \mu\ .\ V / Td \qquad (3)$$

where μ is the viscosity of the ductile layer, V is the shortening rate and Td the thickness of the ductile layer.

A strength profile is built according to these equations in order to define the strength ratio (SR) between the brittle (Sb) and ductile (Sd) strength, e.g. SR = Sb/Sd (Fig. 9).

The ductile layer is often a potential decollement layer. In the case of a weak shortening velocity, Sd is very low and promotes an effective decollement level. Whereas with a high shortening velocity (strong Sd), the ductile layer can not produce a decollement layer (Fig. 10).

Acknowledgements:

The authors thank J.-J. Kermarrec for his valuable technical assistance, and J. Ballard for constructive discussions. We thank Daniel L. Yagupsky for his very detailed review and constructive suggestions that helped us to improve the manuscript. S. Mullin post-edited the English style.

References

Allemand, P., Brun, J.-P., Davy, P. & Van Den Driessche, J. 1989. Symétrie et asymétrie des rifts et mécanismes d'amincissement de la lithosphère. Bulletin de la Société Géologique de France, 3(V), 445-451.

Balé, P. 1986. Tectonique cadomienne en Bretagne nord. Interaction décrochement chevauchement : champs de déformation et modélisations expérimentales. Thèse de 3ème cycle, Université de Rennes 1.

Ballard, J.F., 1989. Approche géologique et mécanique des décollements dans la croûte supérieure Doctorat, Université de Rennes 1, 301 p.

Barrier, L., Nalpas, T., Gapais, D., Proust, J.-N., Casas, A. & Bourquin, S., 2002. Influence of syntectonic sedimentation on thrusts geometry. Field examples from the Iberian Chain (Spain) and analogue modeling. Sedimentary Geology, 146, 91-104.

Bonini, M., 2001; Passive roof thrusting and forelandward fold propagation in scaled brittle-ductile physical models of thrust wedges, J. Geophys. Res., 106, 2291–2311.

Bonini, M., 2003. Detachment folding, fold amplification, and diapirism in thrust wedge experiments. Tectonics, 22, 6, p.1065, doi: 10.1029/2002TC001458.

Casas, A.M., Gapais, D., Nalpas, T., Besnard, K. et Roman Berdiel, T., 2001. Analogue models of transpressive systems. Journal of Structural Geology, 23(5): 733-743.

474 Couzens-Schultz, B., Vendeville, B. and Wiltschko, D., 2003. Duplex style and triangle zone formation:
475 insights from physical modeling. Journal of Structural Geology, 25(10): 1623-1644.

476 Davy, P. & Cobbold, P. R. 1991. Experiments on shortening of a 4-layer model of continental
477 lithosphere. Tectonophysics, 188, 1-25.

478 Dunn, J.F., Hartshorn, K.G. et Hartshorn, P.W., 1995. Structural styles and hydrocarbon potential of the
479 sub-Andean thrust belt of southern Bolivia. In: Petroleum basins of South America. Tankard A.J.,
480 Suárez R. et Welsink H.J. (eds). American Association of Petroleum Geologists Memoir, 62: 523-
481 543.

482 Echavarria, L., Hernandez, R., Allmendinger, R. and Reynolds, J., 2003. Subandean thrust and fold belt
483 of northwestern Argentina: Geometry and timing of the Andean evolution. AAPG Bulletin, 87 (6):
484 965-985.

485 Horton, B.K. 1999. Erosional control on the geometry and kinematics of thrust belt development in the
486 central Andes. Tectonics, 18 (6): 1292-1304

487 Faugère, E. et Brun, J.P., 1984. Modélisation expérimentale de la distension continentale. Comptes-
488 Rendus de l'Académie des Sciences, Série II, 299 : 365-370.

489 Gestain, V., Nalpas, T., Rouby, D. et Barrier, L., 2004. Rôle des niveaux incompétents syncinématiques
490 sur l'évolution des structures chevauchantes. Bulletin de la Société Géologique de France.

491 Krantz, R. W. 1991. Measurements of friction coefficients and cohesion for faulting and fault
492 reactivation in laboratory models using sand and sand mixtures. Tecyonophysics, 188, 203-207.

493 Labaume, P., Moretti, I., 2001. Diagenesis-dependence of cataclastic thrust fault zone sealing in
494 sandstones. Example from the Bolivian Sub-Andean Zone. Journal of Structural Geology, 21,
495 1659-1675.

496 Leturmy, P., Mugnier, J.L., Vinour, P., Baby, P., Colletta, B., Chabron, E., 2000. Piggyback basin
497 development above a thin-skinned thrust belt with two detachment levels as a function of
498 interactions between tectonic and superficial mass transfer: the case of the Subandean Zone
499 (Bolivia), in Tectonophysics 320, 45–67.

500 Malavielle, J. 1984. Modélisation expérimentale des chevauchements imbriqués: application aux
501 chaînes de montagnes, Bulletin de la Société Géologique de France, XXVI(1), 129-138.

502 Massoli, D., Koyi, H. A., Barchi, M. R., 2006. Structural evolution of a fold and thrust belt generated by
503 multiple décollements: analogue models and natural examples from the Northern Apennines (Italy),
504 Journal of Structural Geology, 28, 185–199.

505 Meneley, R., 2006. Exploration in the Parry Islands and Cornwallis Fold Belts : Canadian Arctic, in
506 2006 CSPG – CSEG – CWLS Convention.

Nalpas, T., Györfi, I., Guillocheau, F., Lafont, F. et Homewood, P., 1999. Influence de la charge sédimentaire sur le développement d'anticlinaux synsédimentaires. Modélisation analogique et exemples de terrain (Bordure sud du bassin de Jaca). Bulletin de la Société Géologique de France, 170(5) : 733-740.

Nalpas, T., Gapais, D., Verges, J., Barrier, L., Gestain, G., Leroux, G., Rouby, D., Kermarrec, J.J., 2003. Effects of rate and nature of synkinematic sedimentation on the growth of compressive structures constrained by analogue models and field examples. Geological Society of London Special Publication 208, 307–319.

Smit, J.H.W., Brun, J.-P., Sokoutis, D., 2003.Deformation of brittle-ductile thrust wedges in experiments and nature, in journal of geophysical research, vol. 108, no. B10, 2480, doi: 10.1029/2002JB002190.

Vendeville, B., Cobbold, P., Davy, P., Brun, J.P., et Choukroune, P., 1987. Physical models of extensional tectonics at various scales. In: Continental extensional tectonics. Coward, J.F., Dewey, J.F. et Hancock, P.L. (eds). Geological Society of London Special Publications, 28: 95-107.

Fig.1. (a) Geological map of the central Andean compressive system (after Horton, 1999), and (b) focus geological map of the Bolivian sub-Andean thrust-belt (modified from Dunn et al., 1995). (c) Cross-section of this system (see red line in Fig. 1b for location) showing the main structural organisation (modified from Labaume and Moretti, 2001).

Fig.2. (a) Experimental apparatus and (b) sketch of homogeneous and local synkinematic sedimentation depositions. R is the ratio between the velocity of the sedimentation: Vs, and the velocity of the structure uplift: Vu (R = Vs / Vu, see Barrier et al., 2002).

Fig.3. Cross-sections of experiments for (a) 5 cm of shortening, (b) 1 cm of shortening and (c) 0.5 cm of shortening. S = total shortening and VD corresponds to the Velocity Discontinuity. A thick black line symbolizes the mobile wall and the mobile plate.

Fig.4. Simple cross-sections showing the relationship of the ratio R between sedimentation velocity (Vs) and uplift velocity (Vu) and the base level.

Fig.5. Cross-section of experiments with homogeneous synkinematic sedimentation for (a) column with 5 cm of shortening and (b) column with 10 cm of shortening. The ratio R, between sedimentation velocity (Vs) and uplift velocity (Vu), is related to each experiment presented in the same line. VD corresponds to linear Velocity Discontinuity.

Fig.6. Cross-section of experiments with local synkinematic sedimentation for (a) column with 5 cm of shortening and (b) column with 10 cm of shortening. The ratio R, between sedimentation velocity (Vs) and uplift velocity (Vu), is related to each line of experiment. VD corresponds to linear Velocity Discontinuity.

Fig.7. 3D sketch and strength profiles of the experiments with (a) 5 cm of shortening and without synkinematic sedimentation, (b) 5 cm of shortening and with homogeneous synkinematic sedimentation, and (c) 5 cm of shortening and with local synkinematic sedimentation. The number and letter show the evolution of the deformation.

Fig. 8. Field examples of thrust structures related to two decollement levels, from the Tarija basin (Argentina; modified from Echavarria et al. 2003).

Fig. 9. Strength profiles of our analogue model for a shortening rate ranging from 0.25 to 10 cm/h.

Fig. 10. Plots of relative strength between the lower brittle and lower ductile layers (black line) and between the upper brittle and upper ductile layers (dashed line) for six different shortening rates (ranging from 0.25 to 10 cm/h). SR is the ratio between the brittle (Sb) and ductile (Sd) strength. The background colour domains correspond to whether or not the ductile layer was able to create an effective decollement level.

Table 1. Scaling Parameters.

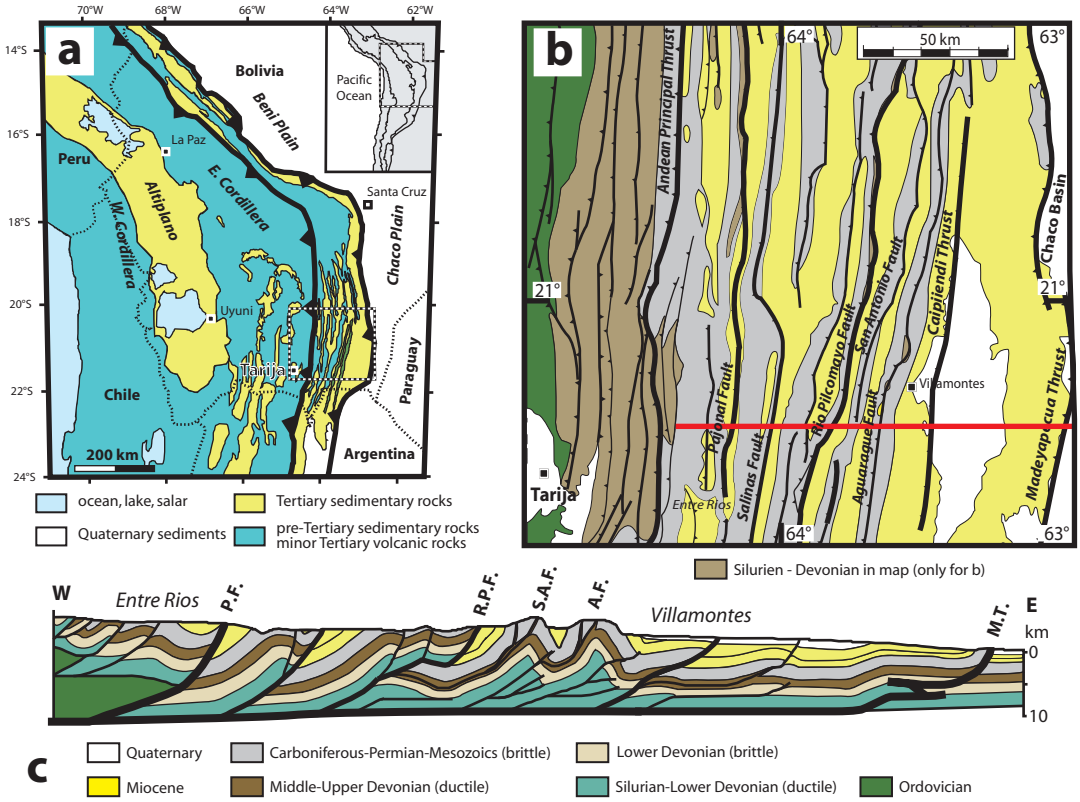
a
70°W
68°W
66°W
64°W
62°W
14°S
16°S
18°S
20°S
22°S
24°S
Bolivia
Peru
Chile
Argentina
Paraguay
La Paz
Uyuni
Tarija
Santa Cruz
Pacific Ocean
Beni Plain
E. Cordillera
Altiplano
W. Cordillera
Chaco Plain
200 km
b
64°
63°
21°
50 km
Andean Principal Thrust
Chaco Basin
Rio Pilcomayo Fault
San Antonio Fault
Calpiendi Thrust
Madeyapecua Thrust
Poñonal Fault
Salinas Fault
Aguaragüe Fault
Villamontes
Tarija
Entre Rios
ocean, lake, salar
Quaternary sediments
Tertiary sedimentary rocks
pre-Tertiary sedimentary rocks
minor Tertiary volcanic rocks
Silurien - Devonian in map (only for b)
W
Entre Rios
P.F.
R.P.F.
S.A.F.
A.F.
Villamontes
M.T.
E
km
0
10
c
Quaternary
Miocene
Carboniferous-Permian-Mesozoics (brittle)
Middle-Upper Devonian (ductile)
Lower Devonian (brittle)
Silurian-Lower Devonian (ductile)
Ordovician

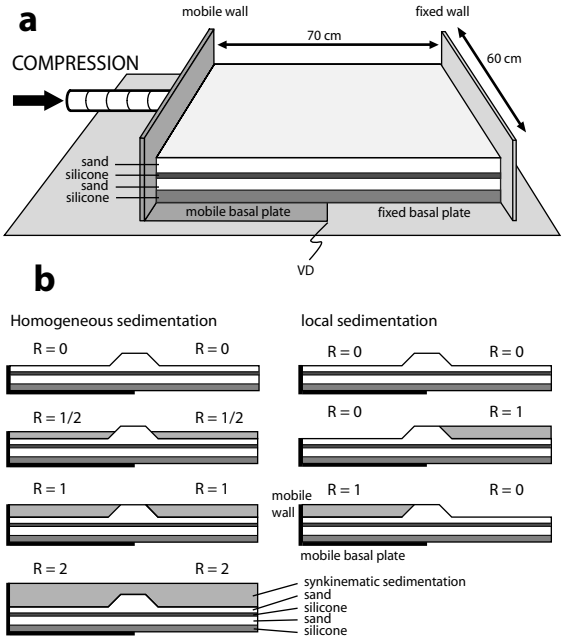
a
mobile wall
fixed wall
70 cm
60 cm
COMPRESSION
sand
silicone
sand
silicone
mobile basal plate
fixed basal plate
VD
b
Homogeneous sedimentation
local sedimentation
R = 0
R = 0
R = 0
R = 0
R = 1/2
R = 1/2
R = 0
R = 1
R = 1
R = 1
mobile wall
R = 1
R = 0
mobile basal plate
R = 2
R = 2
synkinematic sedimentation
sand
silicone
sand
silicone

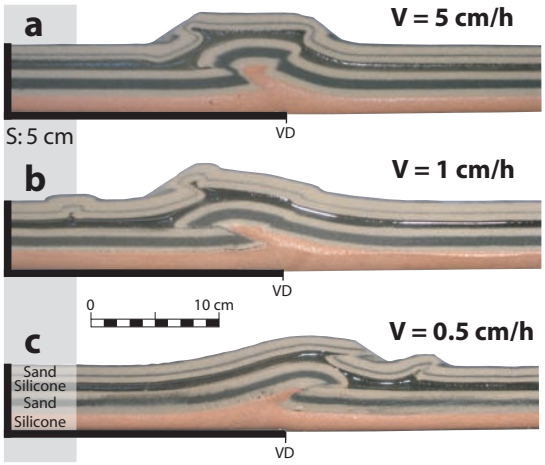
a
V = 5 cm/h
S: 5 cm
VD
b
V = 1 cm/h
VD
0
10 cm
c
V = 0.5 cm/h
Sand
Silicone
Sand
Silicone
VD

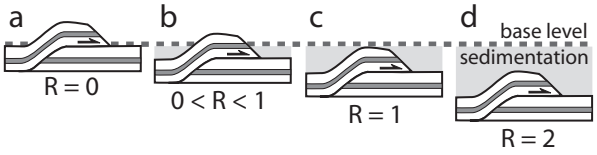
a
b
c
d
base level
sedimentation
R = 0
0 < R < 1
R = 1
R = 2

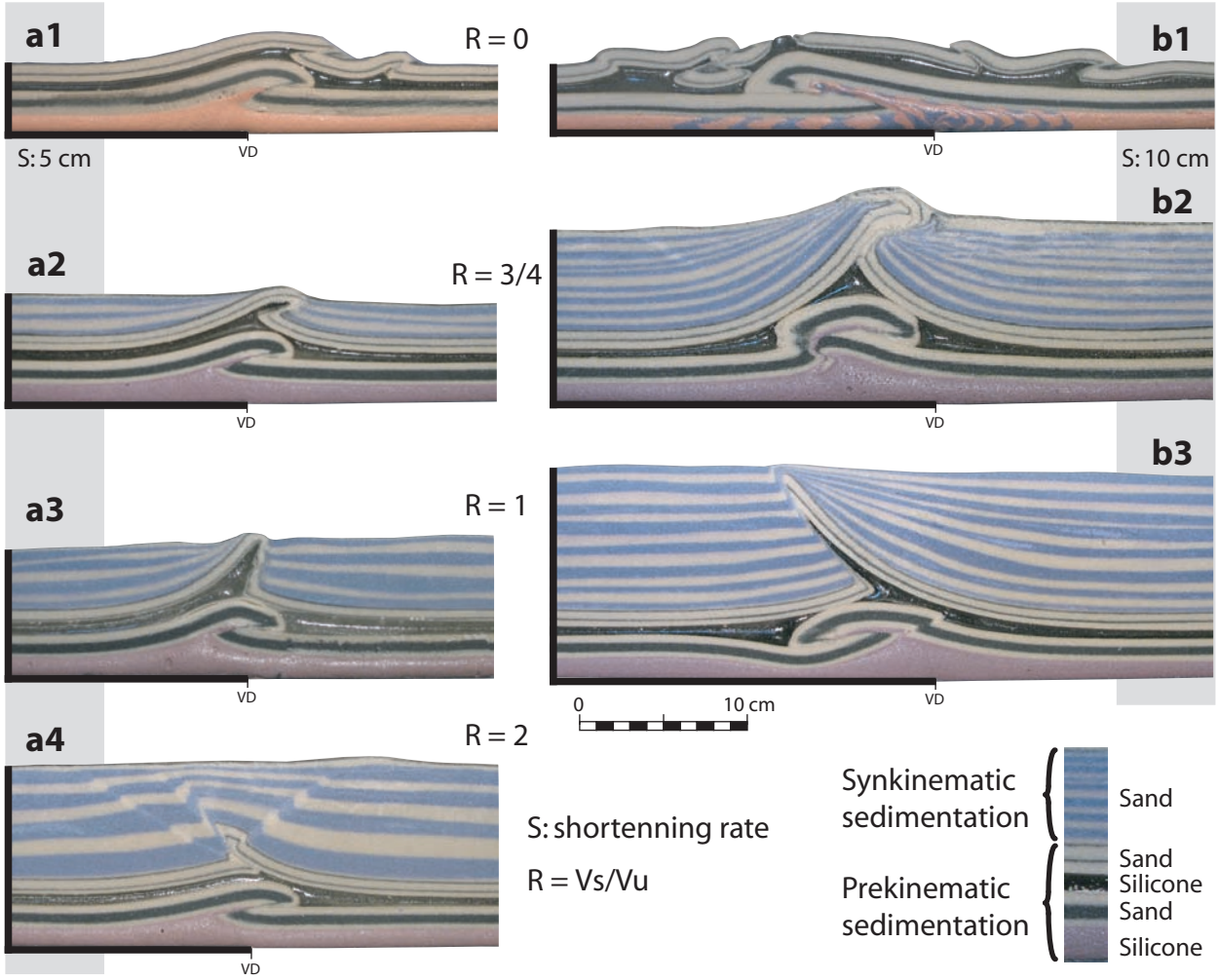
a1
R = 0
b1
VD
VD
S: 5 cm
S: 10 cm
b2
a2
R = 3/4
VD
VD
b3
a3
R = 1
VD
0
10 cm
VD
a4
R = 2
VD
S: shortenning rate
R = Vs/Vu
Synkinematic sedimentation
Sand
Prekinematic sedimentation
Sand
Silicone
Sand
Silicone

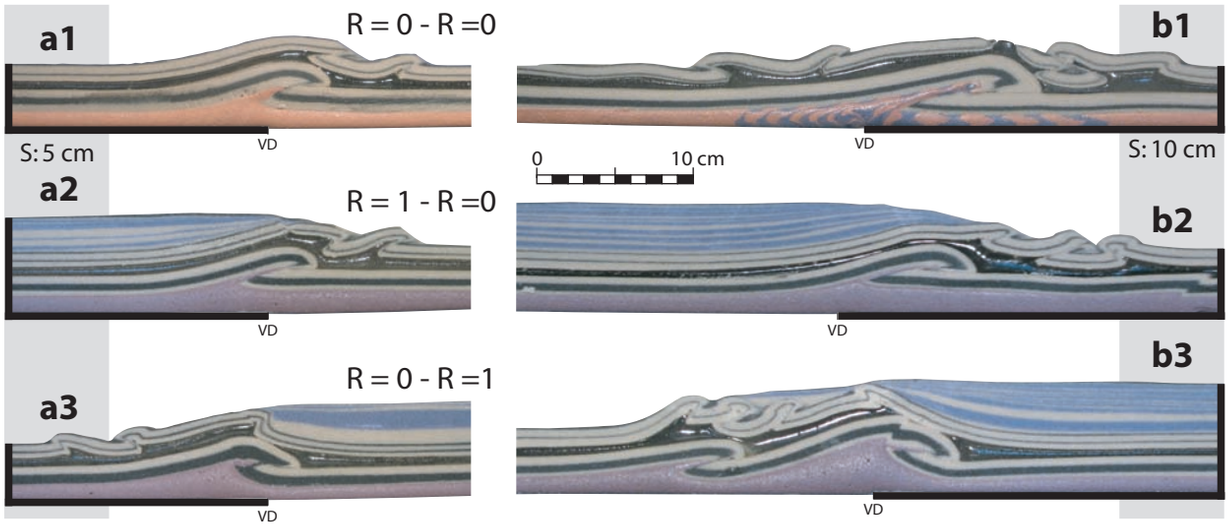
a1
R = 0 - R =0
VD
S: 5 cm
a2
R = 1 - R =0
VD
a3
R = 0 - R =1
VD
0
10 cm
b1
VD
S: 10 cm
b2
VD
b3
VD

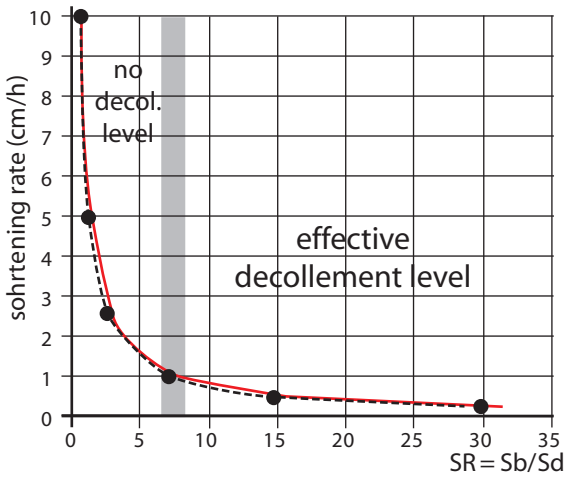
sohrtening rate (cm/h)
10
9
8
7
6
5
4
3
2
1
0
no
decol.
level
effective
decollement level
0
5
10
15
20
25
30
35
SR = Sb/Sd

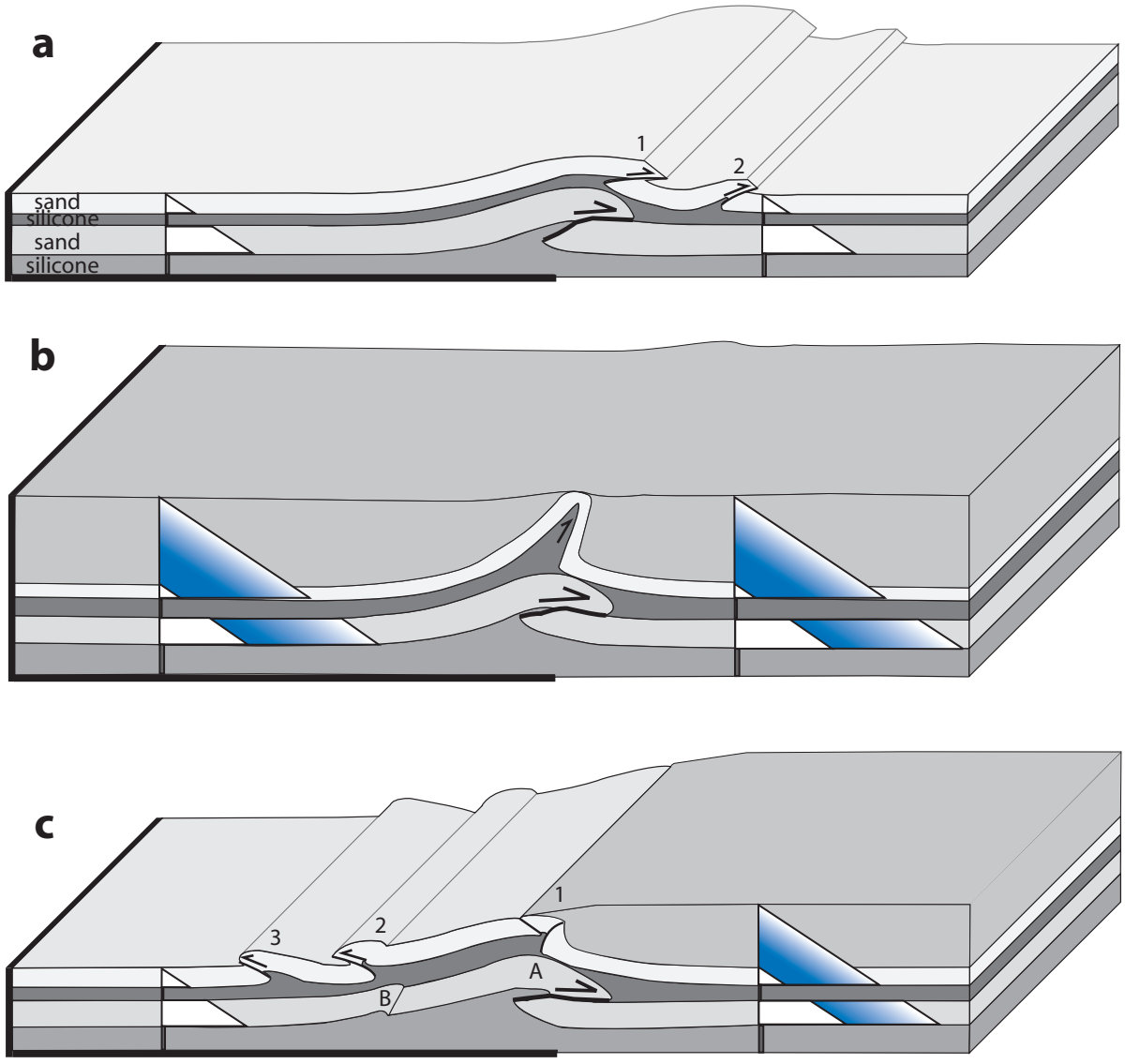
a
1
2
sand
silicone
sand
silicone
b
1
c
1
2
3
A
B

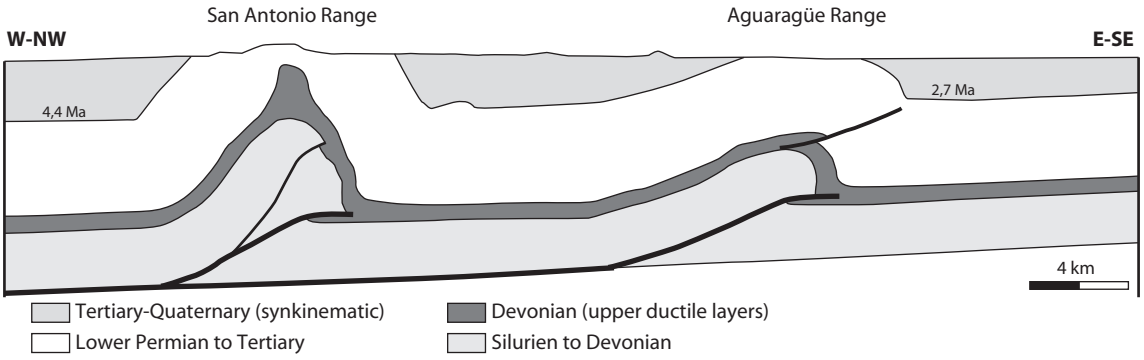
San Antonio Range
Aguaragüe Range
W-NW
E-SE
4,4 Ma
2,7 Ma
4 km
Tertiary-Quaternary (synkinematic)
Lower Permian to Tertiary
Devonian (upper ductile layers)
Silurien to Devonian

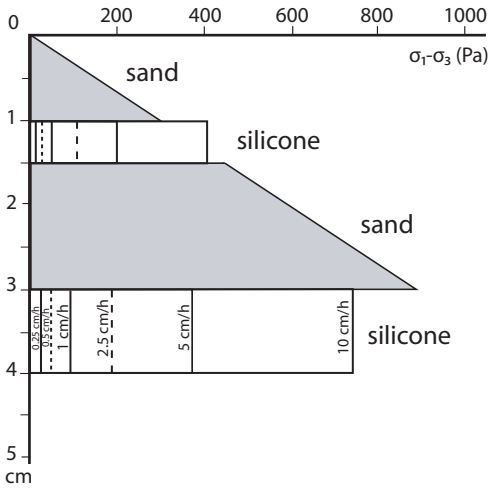
0
200
400
600
800
1000
σ1-σ3 (Pa)
sand
1
silicone
2
sand
3
0.25 cm/h
0.5 cm/h
1 cm/h
2.5 cm/h
5 cm/h
10 cm/h
silicone
4
5
cm

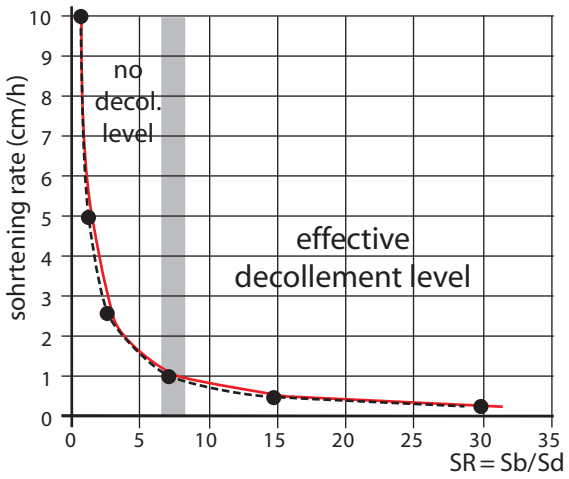
sohrtening rate (cm/h)
10
9
8
7
6
5
4
3
2
1
0
no
decol.
level
effective
decollement level
0
5
10
15
20
25
30
35
SR = Sb/Sd

	L (m)	g (m/s^2)	ρ (kg/m3)	μ (Pa.s)	V (m/s)	t (s)	σ (Pa)
Nature	1000 (1km)	9.81	2300	10^{17} - 10^{19}	$3.2x10^{-10}$ (1 cm/y)	$1.6x10^{13}$ (0.5 Ma)	$2.2x10^{7}$
model	0,01 (1cm)	9.81	1400	10^{4}	$1.4x10^{-6}$ (0.5 cm/h)	$3.7x10^{4}$ (10 h)	$1.5x10^{2}$
model / nature ratio	10^{-5}	1	0.6	10^{-14}	$4x10^{3}$	$2.6x10^{-9}$	$6x10^{-5}$